Particles dissolution and liquid mixing dynamics by Electrical Resistance Tomography

Particles dissolution and liquid mixing dynamics by Electrical Resistance Tomography

A.Paglianti[1*], F. Maluta[1], G. Montante[2]

[1] Dipartimento di Ingegneria Civile, Chimica, Ambientale e dei Materiali, Alma Mater Studiorum – Università di Bologna, Bologna, Italy
[2] Dipartimento di Chimica Industriale "Toso Montanari", Alma Mater Studiorum – Università di Bologna, Bologna, Italy

[*]Email: alessandro.paglianti@unibo.it

ABSTRACT

Salt particles dissolution in slurry stirred tanks provides an ambitious challenge for the application of Electrical Resistance Tomography in the process industry, because the presence of high loadings of inert particles requires a purposely developed post-processing method of the experimental data. For the optimization of the working conditions of the dissolution process, two characteristic times are required: the time for the liquid homogenization in the tank and the time required for the complete dissolution of the salt particles. The former time has been experimentally determined in previous investigations both in stirred tanks working with single-phase and as well as with multiphase mixtures. The latter characteristic time has not been analyzed so far, due to the lack of experimental procedures for distinguishing it from the former. In this work, a novel approach for the simultaneous identification of the two characteristic times is presented. The impact of the new procedure is significant for the production processes, since it offers a tool for identifying when the soluble particle size has an impact on the dissolution dynamics, and when the stirred tank dynamics is influenced by the liquid homogenization only, and therefore a reduction of the particle size doesn't speed up the process accomplishment.

Keywords Electrical Resistance Tomography, Mixing time, Mass transfer, Slurry stirred tanks, Solids dissolution.

NOMENCLATURE

C	impeller clearance, m
C_i	dimensionless conductivity in the pixel i, dimensionless
CoV	coefficient of variation, dimensionless
CoV_{norm}	normalized coefficient of variation, dimensionless
D	impeller diameter, m
d_p	particle volume averaged mean size, μm
H_T	vessel height, m
H_L	liquid height, m

K_i	conductivity in the pixel i, mS/cm
N	impeller speed, rpm
N_p	number of pixels per plane, dimensionless
N_{JS}	just suspended impeller speed s^{-1}
T	vessel diameter, m
t	time, s
z_1,z_2,z_3,z_4	elevations of the measurement planes, m
X	mass ratio of inert solid to liquid, dimensionless

Greek letters

σ_i	dimensionless variance in the pixel i, dimensionless
$\sigma_{norm,i}$	normalized variance in the pixel i, dimensionless
ρ_s	solid density, kg/m^3
χ_i	normalized conductivity in the pixel i, dimensionless
$\bar{\chi}$	mean normalized conductivity, dimensionless

INTRODUCTION

Solid-liquid stirred vessels and reactors are widely used in several industrial processes, such as among others, chemical, mining, food and pharmaceutical sectors. Optimized design of solid-liquid mixing operations in stirred tanks can be obtained by a detailed knowledge of local characteristics of the two-phase flow, such as liquid and solid velocities and solid concentration distribution, and global parameters, as impeller power and flow numbers and mixing time, which change with the vessel geometry and the solid-liquid system properties (Atiemo-Obeng et al., 2004).

Among the industrially relevant applications involving solid-liquid mixing, in this work the dissolution of solids in dense suspensions of inert particles is specifically addressed. In particular, the dissolution dynamics are experimentally observed and two characteristic times are considered: the liquid mixing time and the solids dissolution time. For the investigation, Electrical Resistance Tomography (ERT) is selected, which provides information on several locations simultaneously and is particularly suitable for improving the industrial operations design and optimization (Stanley et al., 2002). Due to the specific features of turbulent solid-liquid flows in stirred tanks, purposely developed post-processing methods are required to extract industrially relevant information from the conductivity data collected by ERT. The conductivity variations due to liquid mixing and solids dissolution are masked by the variations of the inert solid local instantaneous concentration, which are due to the turbulent fluctuations and the impeller rotation.

To date, the effect of the solid concentration on the mass transfer coefficient has not been fully clarified. Harriott (1962) suggested that solid loading has not effect of the mass transfer coefficients, Cline (1978) reported a decrement on mass transfer coefficient increasing the solid concentration, while Bong et al. (2015) found that, if the stirred tank works at the just suspended conditions, the mass transfer coefficient depends from the solid loading in a non-monotonic way. So far, ERT was applied to the investigation of

stirred tanks to measure the solid concentration in dense suspensions (e.g. Hosseini et al., 2010; Carletti et al. 2014; Lassaigne et al., 2016), the effects of solids in gas-liquid stirred tanks (Cooke et al., 2008), the liquid homogenization time using a passive tracer (Carletti et al., 2016; Paglianti et al., 2017a, Sardeshpande et al., 2016) and the liquid homogenization in case of floating particles (Paglianti et al., 2017b). To the best of our knowledge, this is the first investigation addressing particles dissolution in dense solid-liquid stirred tanks based on ERT data, with the partial exception of the work of Shirhatti et al. (2005).

EXPERIMENTS

The salt particles dissolution and the liquid mixing times are investigated in the stirred vessel schematically depicted in Figure 1, where the main components of the ERT instrumentation are also included. The stirred tank consisted in a cylindrical and flat-bottomed vessel of diameter, T, equal to 0.23 and height, H_T, equal to 1.21T. The vessel lateral wall was provided with four equally spaced vertical baffles of width W equal to T/10. The agitation was provided by an axial impeller, that is particularly suitable for solid suspension, a Lightnin A310 impeller (A310) of diameter D equal to 0.41T. The impeller was mounted on a central shaft and placed at distance from the vessel bottom, C, equal to T/3.

The NaCl particles dissolution was carried out in a solid–liquid system consisting in a very dilute aqueous solution of NaCl (salt concentration equal to 0.086 g/L) and glass beads. The vessel was filled with the solid-liquid mixture up to the height H_L=1.08T.

The glass particle, of density, ρ_s, equal to 2500 kg/m^3, were sieved into a narrow size range. The particle size distribution (PSD) was measured by means of a Malvern Mastersizer 3000, based on laser diffraction and the Mie theory. The particle volume averaged mean size, d_p, was equal to 385 μm and the corresponding Sauter diameter was equal to 373 μm. The mass ratio, X, (i.e. kg solid/kg liquid), of the glass particles was equal to 0.43 (corresponding to a solid volume fraction of 0.147). The impeller speed, N, was fixed at 600 rpm in order to investigate an incomplete suspension condition, that is particularly tough, due to the strong inhomogeneity of the solid distribution(Carletti et al., 2014). The glass particles just suspended impeller speed, N_{JS}, which provides a reference value for the achievement of the complete particle suspension, was estimated visually placing a mirror inclined of 45° below the vessel base. Following the well-known Zwietering's just suspended criterion, a value of approximately 830 rpm was measured.

As the dissolving solids, 2 gr of different NaCl grain sizes were adopted, with mean diameters, d_p, equal to 0.42 mm, 1.59 mm and 3 mm. The salt particles were added just above the liquid surface from the top lid of the vessel by a hole placed tangentially at 11.25° downstream a baffle and radially midway between the shaft and the vessel wall.

The salt dissolution dynamics was obtained by the ITS P2000 ERT instrumentation (Industrial Tomography Systems Ltd.), by which the distribution of the electrical conductivity in the horizontal sections of the vessel provided with the electrodes was measured as a function of time. The electrodes were arranged at equal intervals around the wall of the vessel, as shown in Figure 1. The measurement is based on the injection of a current between a pair of electrodes and the determination of the resultant voltage difference between the remaining electrodes.

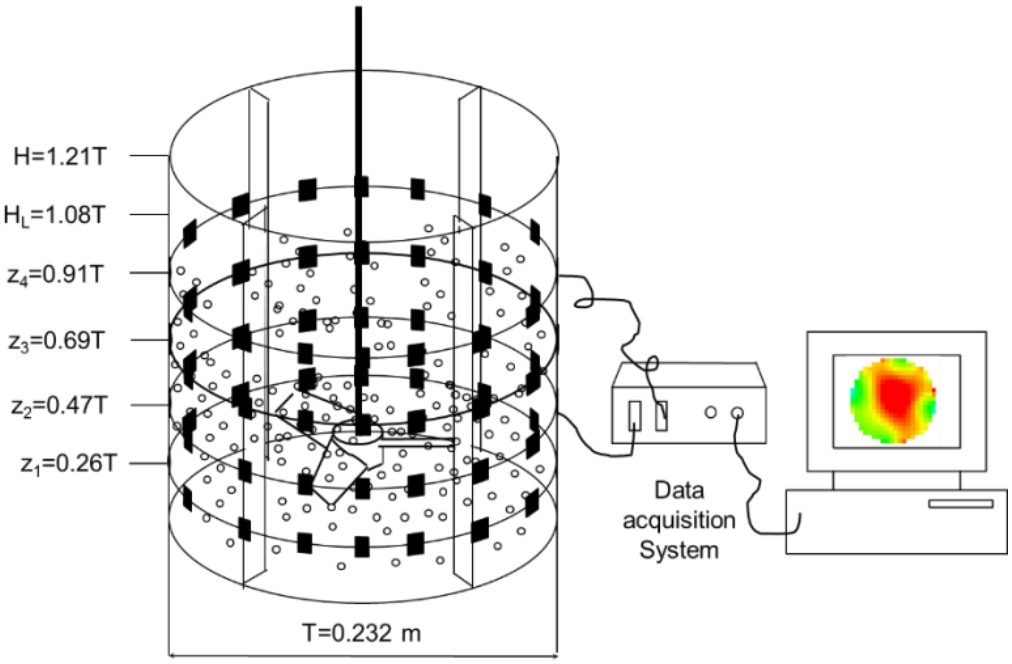

Figure 1. Sketch of the experimental stirred vessel.

The electrodes were connected to the data acquisition system by coaxial cables for reducing the effect of noise and interference. The amplitude of 15 mA and the injected current frequency of 9600 Hz were adopted after preliminary calibration tests. The voltage for each recorded frame was determined by the average of eight instantaneous samples. The number of recorded frames was varied from 1500 to 3000 depending on the total time required for the complete salt dissolution, that was determined by preliminary tests performed for each salt particle size and impeller speed. In all cases, the acquisition was started 20 s before the salt addition. The time resolution of the collected time trace was equal to 0.43 s, resulting from the acquisition of 2.3 frames per second. The selected acquisition rate was fast enough for following the dissolution dynamics in all the investigated conditions. The local conductivity was obtained from the voltage measurements by adopting the linearized back projection algorithm in real time on a square grid of side equal to 11.5 mm. The number of pixels per plane was equal to 316.
The axial elevations of the four horizontal measurement planes, z_i, and the characteristics of the electrodes adopted for the ERT measurements are provided Table 1.
The reliability of ERT for the mixing time determination in single phase stirred tanks is widely accepted (Sarderspande e al., 2016) and the reliability of the technique adopted in this work was specifically verified in a previous investigation (Montante and Paglianti, 2015). The ERT system has been also successful adopted for the measurement of salt dissolution in single phase stirred vessels (Carletti et al., 2018). Additional validation tests are not performed in this work.

Variable	**Value**

Elevation of the measurement planes from the tank bottom	0.06 m, 0.11 m, 0.16 m, 0.21 m
Square electrode side	0.02 m
Electrode thickness	0.001 m
Number electrodes per plane	16

Table 1. Main features of the measurement system.

Procedure for the analysis of the conductivity time traces

Different variables are considered and compared for the determination of the liquid mixing time and the solid-liquid mass transfer time and for observing their variations as a function of the size of the dissolved solids. The limitations of the section averaged conductivity evaluations and the problems associated with the disturbances due to the inert solids fluctuations affecting the local conductivity data were discussed elsewhere (Paglianti et al., 2017a).

It is worth observing that during the solids dissolution the liquid mixing time cannot be estimated with the conventional measurement of the local or global conductivity dynamics after the instantaneous injection of a tracer pulse. For this reason in the following, together with the local conductivity, its spatial variations are considered, with the aim to separately observe the two simultaneous dynamics associated to the solid dissolution and the liquid mixing.

The raw data collected by the acquisition system consist in the dimensionless conductivity in the pixel i, $C_i(t)$, that is the conductivity of the slurry at the generic time t, $K_i(t)$ divided by the conductivity of the medium before the salt particles addition $K_{i,ref}$.

$$C_i(t) = \frac{K_i(t)}{K_{i,ref}} \quad (1)$$

The first variable obtained from the raw data is the normalized local conductivity, $\chi_i(t)$ calculated as:

$$\chi_i(t) = \frac{C_i(t) - C_i(0)}{C_i(\infty) - C_i(0)} \quad (2)$$

where $\chi_i(0)=0$ and $\chi_i(\infty)=1$, being at t=0 the solid salt added to the slurry and at t =∞ the dissolution completed. Since $\chi_i(t)$ is always bounded between 0 and 1, irrespective of the initial and final slurry conductivity values, it is a suitable variable for the estimation of the salt dissolution time, defined as the time required to reach a level of variation of $\chi_i(t)$ within ±(1-x) % of $\chi_i(\infty)$, being x a fixed degree of variation.

The spatial variations of $\chi_i(t)$ are observed by two additional variables.

The section averaged variations of $\chi_i(t)$ are quantified by the coefficient of variation, CoV, on each measurement plane, obtained as follows:

$$CoV(t) = \sqrt{\frac{\sum_{i=1}^{N_p}\left(\frac{\chi_i(t)}{\bar{\chi}(t)}-1\right)^2}{N_p-1}} \quad (3)$$

where N_p is the number of pixels on the plane and $\bar{\chi}$ the mean normalized ~~local~~ conductivity on the plane. The liquid mixing time on each measurement plane can be estimated from the normalized CoV, that is calculated as:

$$CoV_{norm}(t) = \frac{CoV(t)-CoV(\infty)}{CoV(0)-CoV(\infty)} \quad (4)$$

where CoV(0) is the averaged CoV value before the injection of the tracer, CoV(∞) corresponds to the complete homogenization condition at t =∞.

The local spatial variations of $\chi_i(t)$ are observed by the dimensionless variance, $\sigma_i(t)$, defined as:

$$\sigma_i(t) = \sqrt{\left(\frac{\chi_i(t)}{\bar{\chi}(t)} - 1\right)^2} \quad (5)$$

The corresponding normalized local value, $\sigma_{norm,i}(t)$ is:

$$\sigma_{norm,i}(t) = \frac{\sigma_i(t)-\sigma_i(\infty)}{\sigma_i(t=0)-\sigma_i(\infty)} \quad (6)$$

In the following, the three variables will be adopted for the assessment of the effect of the salt particles size and the agitation conditions on the selected dissolution process.

Results

The time series of the section averaged values of $\bar{\chi}(t)$and $CoV_{norm}(t)$ on the upper measurement plane, z_4, during the dissolution of NaCl particles of three different sizes are shown in Figure 2 and Figure 3, respectively. In order to smooth the fluctuations of the raw signals due to the inert particles movement on the plane, a moving window average was applied over 2.6 s (Carletti et al. 2016). The moving window average does not modify appreciably the variables during most of the dissolution process, but it is particularly useful to appreciate their variations towards the end of the dissolution, when the small conductivity variations due to the small amount of additional dissolved particles are masked by the inert particles passage on the plane.

In Figure 2 the two horizontal lines represent the boundary that allows to estimate the dissolution time with a degree of variation, x, of ± 5%. The experimental data show that decreasing the salt particle size, the characteristic time decreases, as expected due to the increment of the available surface area.

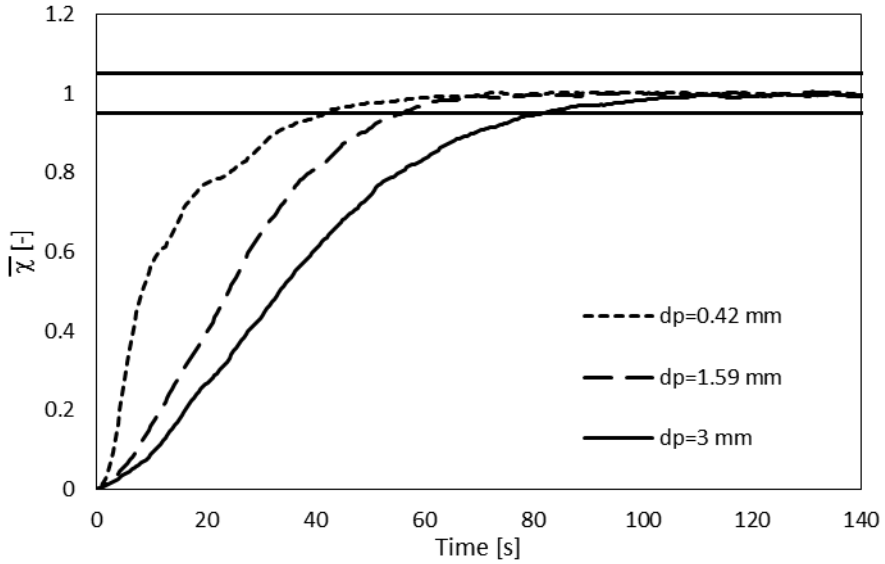

Figure 2. Time traces of the section averaged $\overline{\chi}$ on the measuring plane z_4=0.21m. NaCl particles of d_p equal to 0.42, 1.59 and 3 mm.

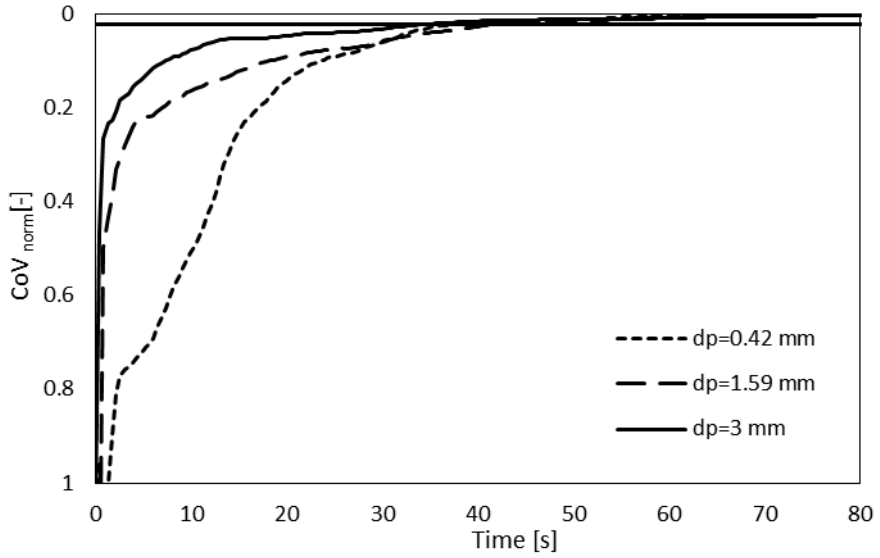

Figure 3. Time traces of the CoV_{norm} on the measuring plane z_4=0.21m. Raw data collected as in Figure 2.

In Figure 3, the threshold CoV_{norm} value of 0.02 suggested by Paglianti et al. (2017a) for the identification of the achievement of the liquid homogenization conditions in slurry stirred tanks is also depicted. The curves shown in Figure 3 evidence that the characteristic time required for the liquid homogenization in the tank is weakly dependent from the particle size. This result has a potential great impact on the design of stirred tanks where the solid dissolution occurs in presence of high solid loadings. In fact, it is interesting to notice that for the larger dissolving particle size (d_p=3 mm), the characteristic time necessary to complete the process, obtained following the time trace

of $\overline{\chi}$, is larger than the homogenization time estimated following the CoV_{norm} experimental trend. Instead, for the tiny particles (d_p=0.42 mm), the two times are practically the same. As a result, the particle size reduction below a critical limit has not any practical effect on the time necessary for the salt dissolution and the homogenization of the mixture.

It is worth observing that this conclusion is based on the time traces of the mean variables on plane z_4, that is, among the four, the plane where the observed phenomena are the slower, as can be clearly appreciated in Figure 4 and 5, where the $\overline{\chi}$ and the CoV_{norm} time traces collected during the 3 mm salt particles dissolution on the four planes are depicted.

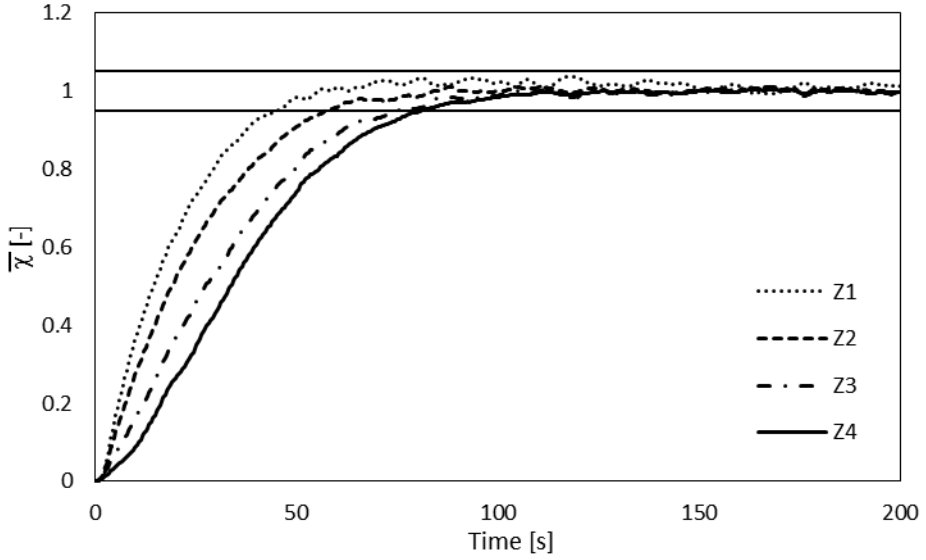

Figure 4. Time traces of the section averaged $\overline{\chi}$ on the measuring planes. NaCl particles of d_p equal to 3 mm.

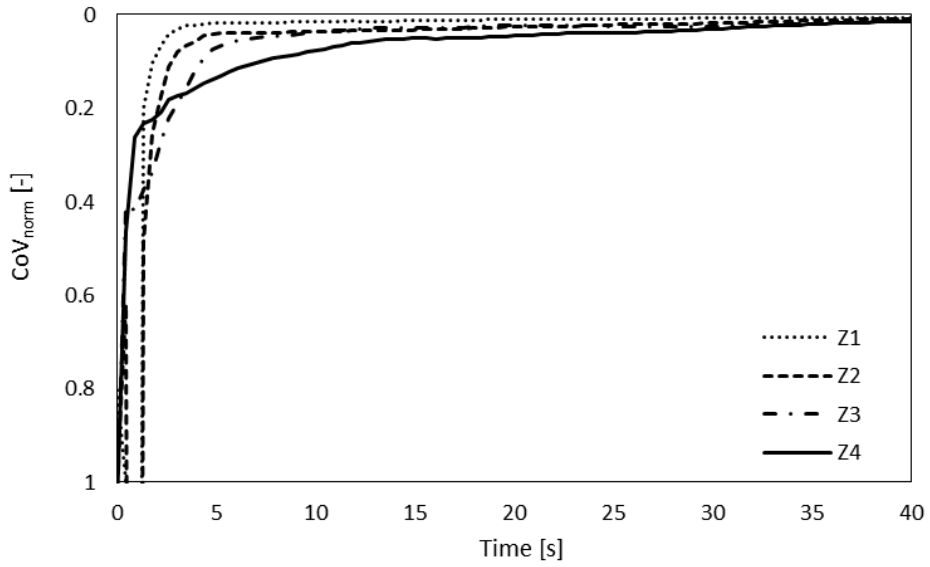

Figure 5. Time traces of the CoV_{norm} on the measuring planes. Raw data collected as in Figure 4.

Clearly the method can be applied to each measurement plane and the procedure repeated to identify the slower zone depending on the impeller speed and the solid suspension features.

The effect of the impeller speed on the salt dissolution dynamics is shown for the case of the 3 mm salt particles in Figure 6. It is worth pointing out that the impeller speed variation significantly affects the amount of suspended inert particles and the particle concentration distribution in the liquid phase, therefore the salt dissolution time experiences a not trivial variation. The just suspended impeller speed, N_{JS}, is equal to about 830 rpm, as estimated visually for the solid-liquid stirred tank under consideration. For $N<N_{JS}$ part of the inert solid is at rest on the tank bottom region. In addition, both above and below N_{JS}, a clear liquid layer can be present in the upper part of the tank. The liquid velocity in this upper clear liquid layer is usually very low, therefore the liquid homogenization time is much slower than in the rest of the vessel volume. The thickness of the clear liquid layer is maximum at N close to N_{JS}, consequently the dissolution time is slower for N=500 rpm and N=900 rpm, while it is faster for N=600-800 rpm.

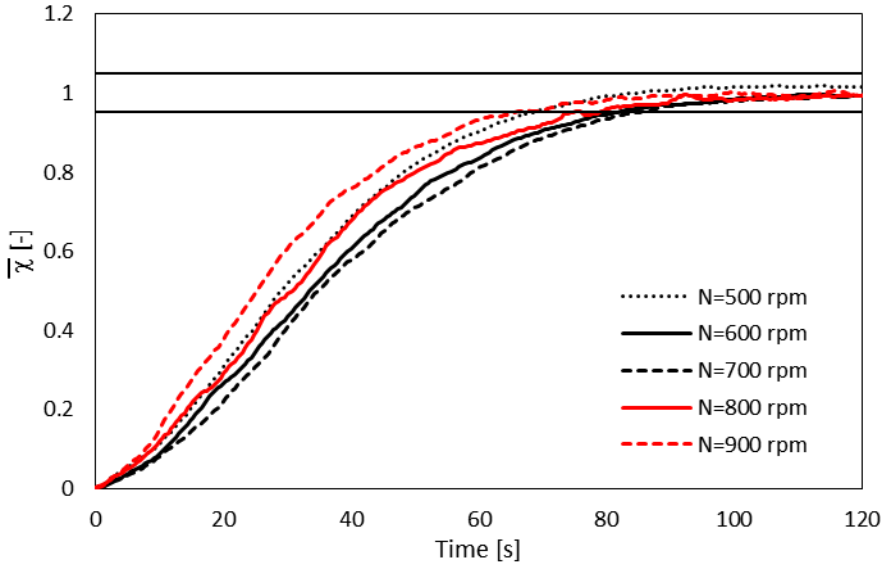

Figure 6. Effect of the impeller speed on the time traces of the section averaged $\overline{\chi}$ on z_4. NaCl particles of d_p equal to 3 mm.

In addition to the analysis of the time evolution of the variables relevant to each single measurement plane, which is already able to provide the very interesting industrial information discussed above, the collected ERT variable can be further exploited on a local basis.

To this end, the values of the local variables estimated in each single pixel are considered. The pixels that fulfil a specific criterion are summed up cumulatively, extending the approach already devised in a previous investigation concerning the suspension of solid particles in stirred vessels (Paglianti et al., 2017a; Paglianti et al., 2017b). Specifically, when the normalized local conductivity, χ_i , is considered, the pixel is assumed to be well mixed using a threshold x of ±0.1. Therefore, when χ_i is in the range 0.9-1.1, the process that is responsible for the conductivity increment, that is the salt dissolution, is assumed completed. The comparison between the results obtained by

the plane averaged variable and the method applied to the same variable on a local basis is depicted in Figure 7. As can be observed, the time trace of the plane averaged $\overline{\chi}$ and the percent number of well mixed pixels reach the asymptotic value in about the same time of 80 seconds from the salt addition. The dynamic behaviour of the two curves is clearly different, because at the beginning the medium conductivity increases, but in none of the pixels the dimensionless conductivity is in the range 0.9-1.1. When the dissolution approaches the end, that is about after 60 seconds, the number of the well mixed pixels sharply increases.

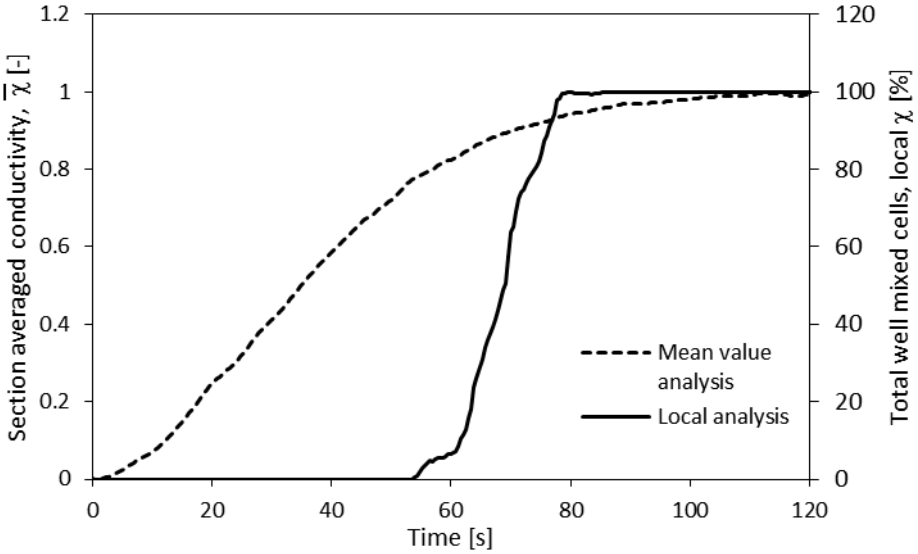

Figure 7. Comparison between the $\overline{\chi}$ time trace and the percentage of well mixed pixels obtained from the local value of χ_i, measuring plane z_4. NaCl particles of d_p= 3 mm.

A similar comparison is performed in Figure 8, using the local and the plane averaged spatial variations of the conductivity, that are obtained by σ_{norm} and CoV_{norm} respectively. When the normalized local variance, σ_{norm}, is considered, the pixel is assumed to be well mixed for a value of σ_{norm} lower or equal to 0.2. In this case, the curves obtained with the two methods are practically overlapped and their trends are different from those plotted in Figure 7. This is because both the variables are associated to the homogeneity condition on the plane and their values can be very low even if the dissolution process is far from being completed.
Overall, the variables and their treatment methods, as shown in Figures 7 and 8, allow to obtain from a single ERT measurement very useful information for optimizing the working conditions of the equipment adopted for dissolution.

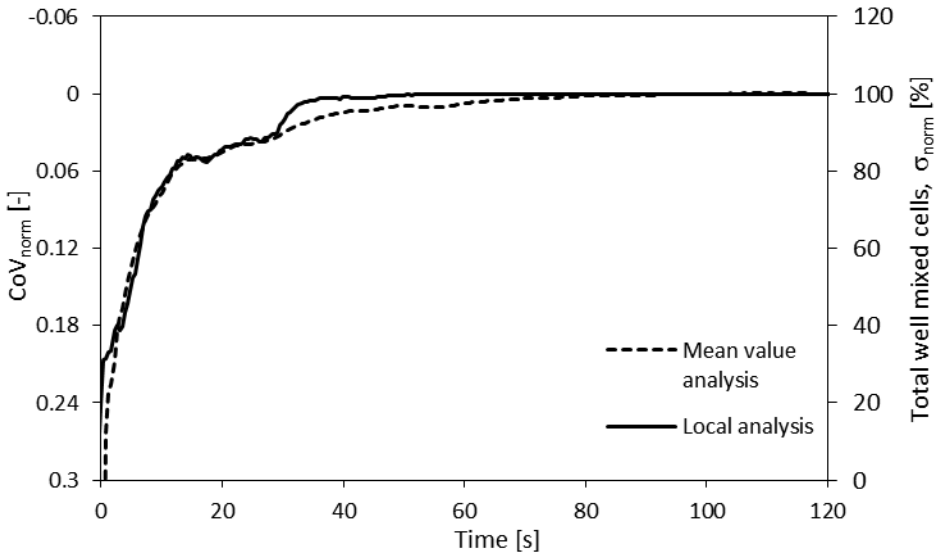

Figure 8. Comparison between the time trace of CoV_{norm} and the percentage of well mixed pixels obtained from the local value of σ_{norm}, measuring plane z_4. NaCl particles of d_p= 3 mm.

The process fallout

A possible outcome of the ERT raw data analysis is the optimization of the dissolution process conditions, which include the impeller speed of the stirred tank, the power consumption and the dimensions of the dissolving particles ensuring the feaster dynamics of both the particle dissolution and the liquid homogenization. In the following, the results obtained by the methods developed in this work, either based on the mean ($\overline{\chi}$ and CoV_{norm}) and the local variables (χ_i and σ_{norm}) will be considered and applied to the identification of the optimal particle diameter for the salt dissolution at the fixed impeller speed, N, of 600 rpm.

The dissolution and the liquid mixing times estimated from the mean variable analysis are shown in Figure 9. For each condition, the time is estimated on the four measurement planes and the maximum value, that always corresponds to that measured on z_4, is plotted. The data corresponding to the particle diameter equal to zero have been collected injecting an aqueous solution of NaCl, without any solid particle inside. Keeping in mind that the liquid mixing time is estimated from the CoV_{norm} analysis and the dissolution time from the $\overline{\chi}$ analysis, the results show that for particles smaller than 1.5 mm, the characteristic times required for the liquid homogenization and the solid dissolution are practically the same, while for larger particles the dissolution is significantly slower than the homogenization. Therefore, it is clear that, once the reactor geometrical characteristics and the impeller speed are fixed, reducing the particle size below a critical value is useless, because the overall time of the process does not change. In the specific case analysed in this work, a reduction of the salt diameter below the 1.5 mm would increase only the mill cost, without changing the total time required for obtaining the homogenization of the mixture.

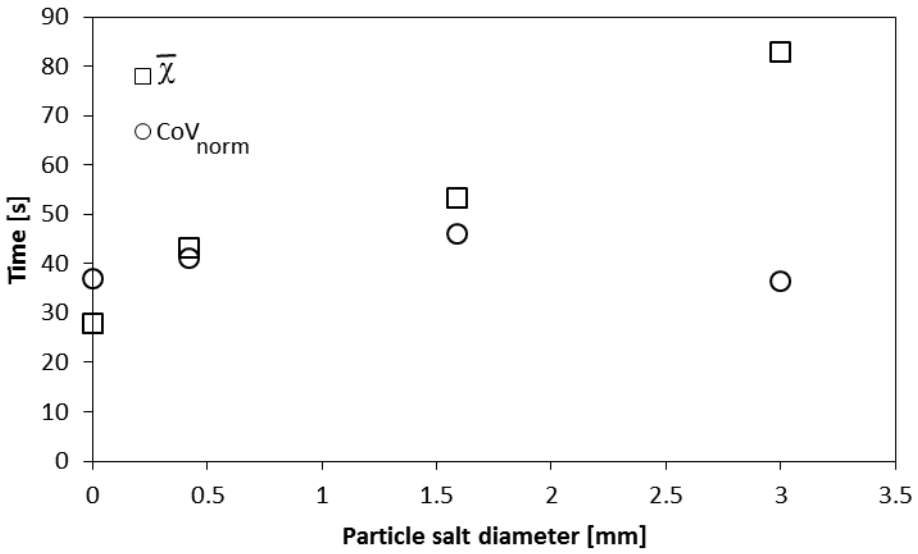

Figure 9. Comparison between the process characteristic times.

The evaluation methods based on the local variables are particularly suitable for the analysis of the dissolution process in stirred suspensions with high loadings of inert particles. For this kind of processes, the equipment fluid dynamics is very complex. The presence of the inert solid phase can hide or distort the identification of the conductivity variations due to the mass transfer phenomena during the dissolution processes. The data post-processing method, based on the local analysis of the dimensionless conductivity or of its variance, allows identifying the total time required for the dissolution. In addition, the tank regions where the dissolution and the liquid homogenization exhibit a different dynamic behaviour or the regions where the processes are slower, as is for example to upper vessel zone in the particular case examined in this work, can be localized. The experimental percentage of perfectly mixed pixels based on the two local variables are shown in Figure 10 as a function of time.

The results indicate that in about 70 seconds the totality of the pixels in the tank appears as well mixed (σ_{norm} criterium), while for obtaining the total dissolution of the salt particles about 80 seconds are required (χ criterium).

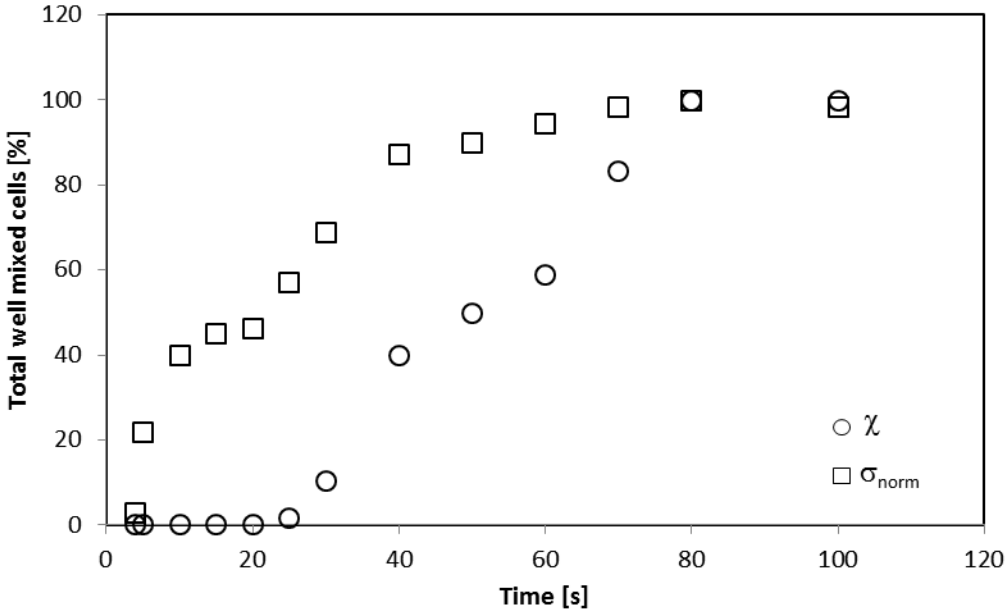

Figure 10. Analysis on the local χ and σ_{norm} values. Percentage of perfectly mixed, dissolution of NaCl particles, d_p=3 mm.

The data shown in Figure 10 practically confirm the conclusion obtained from the mean values analysis.

The local and the mean χ analyses lead to the same conclusions, since both of them identified the characteristic time of 80 s for the process accomplishment. Instead, different values are obtained from the local analysis of σ with respect to the CoV, since the latter leads to the identification of a characteristic time of about 40 seconds, while from the former 70 seconds are required.

The local variables analysis can be also exploited for observing the time evolutions of the well mixed pixels, shown as an example in Figure 11 and in Figure 12, where the results obtained from χ_i and σ_{norm} are reported, respectively.

It can be observed that at the selected impeller speed, the presence of the suspended solid phase divides the stirred tank in two different zones. In the lower zone (z_1 and z_2 planes), because of the impeller effect, the liquid mixing is quite effective and after 60 s the dimensionless conductivity reaches the asymptotic value practically in all the pixels. In upper part of the tank (z_3 and z_4 planes) the fluid is almost at rest and the salt dissolution is very slow, therefore the asymptotic value is reached in about 80 seconds.

The analysis of the σ_{norm} parameter gives other interesting information. In the upper part of the tank, the conductivity gradients, that increase the σ_{norm} values, decrease sharply and after about 20 seconds they are negligible.

The lower part of the tank presents a different behaviour, the σ_{norm} value remains high, and therefore the percentage of the well mixed pixels remains low, until about 40 seconds. Afterwards, the radial gradients are practically negligible in the whole tank.

The observed maps suggest that if the solid phase is not perfectly homogenized, that is a usual working condition for avoiding high energy consumption, the dissolution process

starts in the lower part of the tank, where the radial gradient are initially high. For the experimental conditions considered here, this behaviour lasts for about 20 seconds.

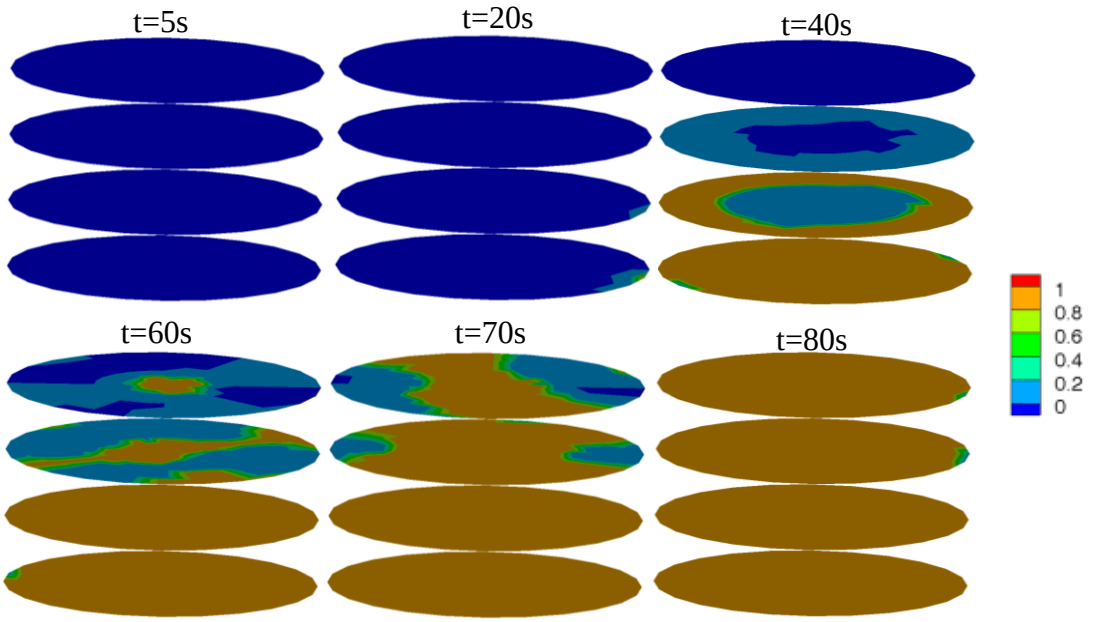

Figure 11. Analysis on the local dimensionless conductivity. Percentage of well mixed pixels, NaCl particles, d_p=3 mm.

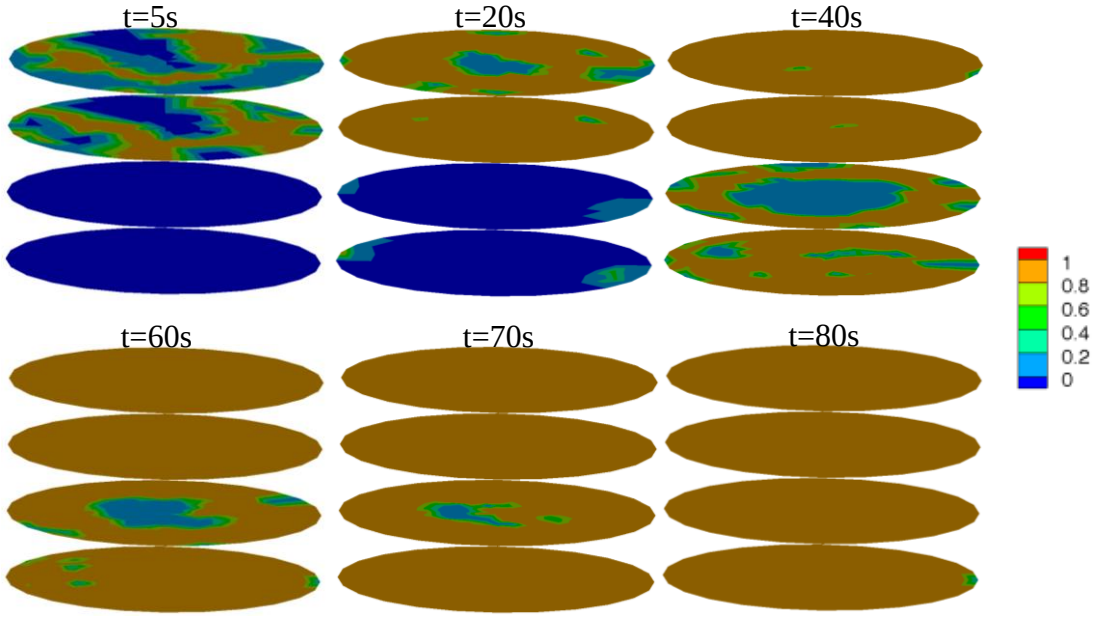

Figure 12. Analysis on the local σ_{norm}. Percentage of well mixed pixels, NaCl particles, d_p=3 mm.

After the start-up period, the conductivity in the lower part of the tank approaches the asymptotic value, while in the upper part of the tank it remains low and it increases slowly because just diffusion processes take place. This second step is completed after at

about 80 seconds. It is interesting to notice that the liquid mixing process in the upper part of the tank appears to be completed after about 20 seconds, as shown from the σ_{norm} analysis on the planes.

CONCLUSIONS

In this work, ERT was successfully applied to the analysis of a salt dissolution process in a vessel stirred by an A310 impeller in presence of a solid-liquid mixture characterized by high loading of inert particles. A particular condition of agitation is selected, which corresponds to the partial suspensions of the inert solids, giving rise to significant salt axial concentration gradients between the lower part of the vessel, where the action of the impeller is important, and the upper part, where the fluid is practically stagnant. The conductivity data provide information both on the homogenization and the dissolution processes. The analysis shows that the ERT raw data can be processed for obtaining different variables of interest, providing a way to separately evaluate liquid mixing and solid dissolution, thus providing a useful tool for the optimization of industrial operations. The dimensionless conductivity and its local/mean variance allows to estimate the dissolution and the homogenization time, respectively.
The analysis of the local values of the variance and of the dimensionless conductivity allows to characterize the mass transfer occurring in the tank. In particular, it is possible to clearly identify if the salt dissolution and liquid mixing occur homogeneously or if zones with a different dynamics are present in the tank. Moreover, the analysis of the local variables allows to identify the zones where the liquid mixing is slower and the planes where the concentration gradients persist for longer time.

REFERENCES

Atiemo-Obeng V A, Penney W R, Armenante P, (2004) Solid–Liquid Mixing, in Handbook of Industrial Mixing: Science and Practice (Eds: E. L. Paul, V. A. Atiemo-Obeng, S. M. Kresta), Wiley-Interscience, ISBN: 0-471-26919-0.

Bong E Y, Eshtiaghi N, Wu J, Parthasarathy R, (2015) Optimum solids concentration for solids suspension and solid-liquid mass transfer in agitated vessels. Chem. Eng. Res. Des., 100, 148-156. DOI:10.1016/j.cherd.2015.05.021.

Carletti C, Montante G, Westerlund T, Paglianti A, (2014) Analysis of solid concentration distribution in dense solid-liquid stirred tanks by electrical resistance tomography, Chem. Eng. Sci. 119, 53-64. DOI:10.1016/j.ces.2014.07.049.

Carletti C, Montante G, De Blasio C, Paglianti A, (2016) Liquid mixing dynamics in slurry stirred tanks based on electrical resistance tomography, Chem. Eng. Sci. 152, 478-487. DOI: 10.1016/j.ces.2016.06.044.

Carletti C, Bikic S, Montante G, Paglianti A, (2018) Mass transfer in dilute solid−liquid stirred tanks, Ind. Eng. Chem. Res. 57, 6505-6515. DOI: 10.1021/acs.iecr.7b04730.

Cline H B A, (1978) Correlation for predicting the mass transfer coefficient in agitated vessels that accounts for the effect of solids concentration on the particle slip velocity. University of Maryland, Maryland, USA.

Cooke, M., Heggs, P.J., Rodgers, T.L (2008) The effect of solids on the dense phase gas fraction and gas-liquid mass transfer at conditions close to the heterogeneous regime in a mechanically agitated vessel. Chem. Eng. Res. Des. 86, 869-882. DOI: 10.1016/j.cherd.2007.10.022

Harriott P, (1962) Mass transfer to particles: Part I. Suspended in agitated tanks, AIChE J., 8, 93-101.DOI: 10.1002/aic.690080122.

Hosseini S, Patel D, Ein-Mozaffari F, Mehrvar M, (2010) Study of solid–liquid mixing in agitated tanks through electrical resistance tomography, Chem. Eng. Sci. 65, 1374-1384. DOI: 10.1016/j.ces.2009.10.007.

Lassaigne M, Blais B, Fradette L, Bertrand F, (2016) Experimental investigation of the mixing of viscous liquids and non-dilute concentrations of particles in a stirred tank, Chem. Eng. Res. Des. 108, 55-68. DOI:10.1016/j.cherd.2016.01.005.

Montante G, Paglianti A, (2015) Gas hold-up distribution and mixing time in gas-liquid stirred tanks, Chem.Eng. J. 279, 648-658. DOI: 10.1016/j.cej.2015.05.058.

Paglianti A, Carletti C, Montante G, (2017a) Liquid Mixing Time in Dense Solid-Liquid Stirred Tanks, Chem. Eng. Tech. 40(5), 862-869 DOI: 10.1002/ceat.201600595.

Paglianti A, Carletti C, Busciglio A, Montante G, (2017b) Solid distribution and mixing time in stirred tanks: The case of floating particles, Can. J. Chem. Eng. 95(9), 1789-1799. DOI:10.1002/cjce.22854.

Shirhatti V, Wang M, Williams R A, (2005) Visualisation of dispersion, dissolution and settling of powders in stirred mixing vessel by electrical resistance tomography, ISIPT 4th World Congress in Industrial Process Tomography, Aizu, Japan, p 474-479.

Sardeshpande M V, Kumar G, Aditya T., Ranade V V (2016) Mixing studies in unbaffled stirred tank reactor using electrical resistance tomography. Flow Meas. Instrum. 47, 110-121. DOI: 10.1016/j.flowmeasinst.2016.01.003.

Stanley SJ, Mann R, Primrose K (2002) Tomographic imaging of fluid mixing in three dimensions for single-feed semi-batch operation of a stirred vessel. Chem. Eng. Res. Des. 80, 903-909. DOI: 10.1205/026387602321143453